Materials Research Bulletin 45 (2010) 474–480

Contents lists available at ScienceDirect

Materials Research Bulletin

journal homepage: www.elsevier.com/locate/matresbu

The competition growth of ZnO microrods and nanorods in chemical bath deposition process

Zhan Yang [a], Yuan-Yuan Shi [a], Xi-Lian Sun [a], Hong-Tao Cao [a,*], Huan-Ming Lu [b], Xu-Dong Liu [c]

[a] Division of Functional Materials and Nano Devices, Ningbo Institute of Material Technology and Engineering, the Chinese Academy of Sciences, Ningbo 315201, People's Republic of China
[b] The Analysis and Testing Division, Ningbo Institute of Material Technology and Engineering, the Chinese Academy of Sciences, Ningbo 315201, People's Republic of China
[c] Shenyang Institute of Engineering, Shenyang 110136, People's Republic of China

ARTICLE INFO

Article history:
Received 9 June 2009
Received in revised form 23 October 2009
Accepted 10 November 2009
Available online 13 November 2009

Keywords:
A. Oxides
A. Nanostructures
B. Chemical synthesis
D. Microstructure

ABSTRACT

Well-aligned ZnO nanorod arrays were synthesized on the *c*-axis orientated ZnO seed layer by chemical bath deposition (CBD) technique. Randomly distributed ZnO microrods with big diameter and growth speed were also formed simultaneously in the same process. The growth of the microrods followed the expected diffusion-limited Ostwald ripening mechanism reasonably well, while that of the nanorods was suggested to be controlled not only by the nutrition ions available but also by the density of nuclei site and the reaction kinetics on the growing surfaces, etc. The microstructure and optical properties of the well-ordered nanorod were also investigated.

1. Introduction

ZnO is a direct wide bandgap semiconductor that crystallizes in hexagonal wurtzite structures [1]. Because of its large exciton binding energy (60 meV), ZnO becomes an ideal material in optoelectronic applications [2]. Along with device miniaturization, quasi-one-dimensional (1D) ZnO nanostructures, such as nanotubes [3], nanobelts [4], and nanorods [5], have attracted extensive interests due to their excellent optical, electrical, gas-sensing, and piezoelectric properties [6–9]. In order to explore the novel nanodevices, such as nanorod-polymer blend solar cells, easily pick up 1D nanostructure and well-defined low dimensional transistor, and so on, it is desirable to obtain well aligned rather than randomly orientated ZnO nanostructures on a cheap complementary metal-oxide semiconductor (CMOS) compatible substrate.

However, it is not easy to prepare the aligned ZnO nanostructures directly on Si substrate due to large differences in thermal expansion coefficients and a considerable lattice mismatch between them. Up to date, well-ordered quasi-1D ZnO nanostructures have been prepared by various methods such as chemical bath deposition (CBD), molecule beam extension, oxidizing the Zn nanowire arrays, chemical vapor deposition, electrodeposition from aqueous solutions, and so on [10–15]. Among these methods, CBD is one of the most convenient and effective methods for the growth of 1D ZnO crystals because of the simple experimental procedures as well as the various ZnO nanostructures harvesting benign. It is well known that a large quantity of zinc hydroxide and zinc oxide precipitates will be formed during the CBD process. These precipitates will then yield crystals following either homogeneous or heterogeneous crystallization mechanism [16–18]. However, it is still unclear how this two growth mechanisms compete with each other.

In this paper, we report a simple two-step solution-phase method, including a sol gel and spin-coated seed layer process and a subsequent CBD process, with a character of low growth temperature, low cost, catalyst free, easy scale-up, high yield, to synthesize ZnO nanostructures. The function of the introduced seed layer and growth mechanisms of ZnO microstructures and nanostructures were also compared and investigated in detail.

2. Experimental

ZnO seed layer was prepared on Si substrate by the sol–gel and spin-coating method. The sol was prepared using a mixed solution of zinc acetate dehydrate, 2-methoxyethanol and monoethanolamine (MEA). The ratio of MEA to ZnO source was maintained at 1.0 and the concentration of Zn in the solution was 0.5 M. The mixed solution was stirred at room temperature for 3 h and then aged over 24 h to form the homogeneous and stable colloid. Prior to coating, the Si (1 0 0) wafers were rinsed in sequence with acetone, methanol, de-ionized (DI) water, solution A (H_2SO_4:H_2O_2:H_2O = 1:1:6),

* Corresponding author. Tel.: +86 57486683486; fax: +86 57486685163.
E-mail address: h_cao@nimte.ac.cn (H.-T. Cao).

0025-5408/$ – see front matter © 2009 Elsevier Ltd. All rights reserved.
doi:10.1016/j.materresbull.2009.11.005

solution B (HF:H_2O = 1:1) and DI water. Eventually the cleaned substrates were dried in nitrogen gas. The ZnO sol was spin coated on the cleaned Si wafers by rotating at 600 rpm for 9 s and then 3000 rpm for 20 s. The prepared films were dried at 350 °C, 400 °C, and 450 °C for 10 min respectively, and finally annealed at 700 °C, 750 °C, and 850 °C for 2 h in air. The substrates with or without seed layer were immerged in an aqueous solution of zinc acetate (0.025 M) and hexamethyleneimine (HMT, 0.025 M). The beaker with the nutrition solution was put into a flume with a constant temperature of 90 °C. After 2 h, the wafers were rinsed with DI water to eliminate residual salts, and dried in air. For comparison studies, the substrates were inserted into the solution with the seed layer face up, face down, or vertically standing configurations. All of the reagents used in this study were in received form without further purification.

Crystal structures were monitored by X-ray diffraction (XRD) θ–2θ scans via D8 Advance spectrometer of Bruker AXS (Germany) with Cu Kα (λ = 1.5419 Å) radiation. The ω scans were recorded with D8 Discover spectrometer Bruker AXS (Germany) with Cu $K\alpha_1$ (λ = 1.5406 Å) radiation. Sample morphologies were observed by field emission scanning electron microscopy (FESEM) (S-4800, Hitachi, Japan) operated at an accelerating voltage of 2.0 kV. Optical absorbance was recorded by a UV-Vis-NIR spectrophotometer (LAMBDA950, PerkinElmer, America). Size of the particles formed in solutions was examined by micro-scale laser particle size analysis instrument (Microtrac S3500). (HR)TEM images, selected area electrical diffraction (SAED) patterns of the nanostructures were taken with a Philips TecnaiG^2 F20 transmission electron microscopy at an accelerating voltage of 120.0 kV. Inductively coupled plasma (ICP) elemental analysis system (Optima2100, PerkinElmer, America) was used to detect the trace contaminations present in the reagents. Photoluminescence (PL) spectrum was excited with a laser (325 nm, 2 mW) at room temperature by Jobin Yvon LABHR UV-NIR spectrometer.

3. Results and discussion

The fabrication of ZnO thin films on Si (1 0 0) underwent the following three procedures: spin coating of ZnO gels, drying, and annealing. Fig. 1(a) shows the XRD patterns of ZnO films annealed at three different temperatures (700 °C, 750 °C, and 850 °C) after dried at 400 °C. While Fig. 1(b) shows the XRD patterns of the films dried at 350 °C, 400 °C, and 450 °C respectively, and then annealed at 750 °C. The intensive peaks close to 34.6° are assigned to (0 0 0 2) reflection of wurtzite ZnO (JCPDS card 36-1451), indicating that all the films are highly oriented with their crystallographic *c*-axis perpendicular to the substrate. The other diffraction peaks can be indexed to the silicon wafer.

Table 1 summarizes the results from XRD patterns of the three dry temperatures (350 °C, 400 °C, and 450 °C) and annealing temperatures (700 °C, 750 °C, and 850 °C). The diffraction peak of (0 0 0 2) is especially obvious and its peak intensity is denoted as $I_{(0\,0\,2)}$. The mean grain size can be calculated by Scherrer's formula:

$$D_m = \frac{0.9\lambda}{\beta \cos\theta}, \tag{1}$$

where D_m is the mean grain size, β is the full-width at half maximum (FWHM) of a distinctive peak (rad, in radian unit), θ is the Brag angle, and λ = 1.5406 Å (Cu Kα).

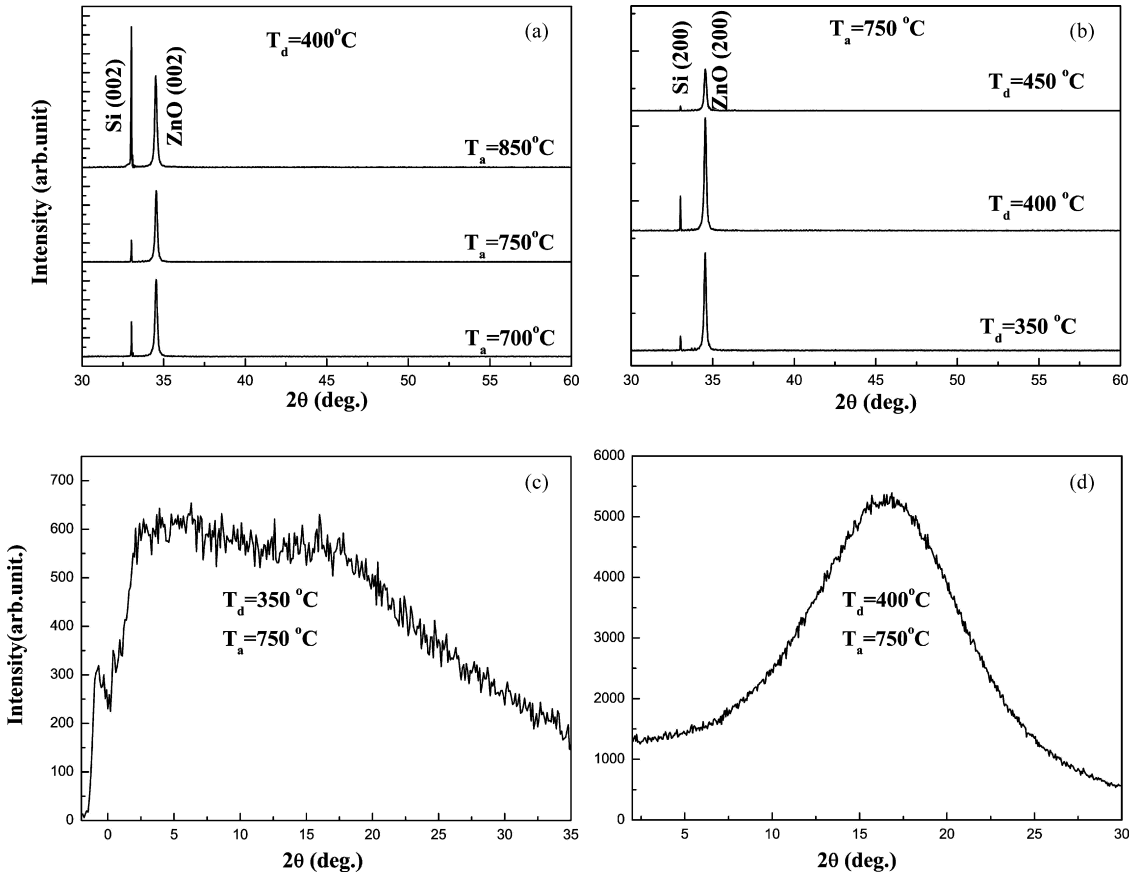

Fig. 1. (a) XRD patterns of ZnO films dried at 400 °C, annealed at 700 °C, 750 °C, 850 °C for 2 h. (b) XRD patterns of films dried at 350 °C, 400 °C, and 450 °C, then annealed at 750 °C for 2 h. (c) X-ray Omega rocking curve of the film dried at 350 °C and annealed at 750 °C. (d) X-ray Omega rocking curve of the film dried at 400 °C and annealed at 750 °C.

Table 1
The crystallinity of sol–gel ZnO thin films of different heat-treatment conditions characterized by the (0 0 0 2) peak.

Sample	Heat-treatment conditions (°C)		2θ (°)	$I_{(0\,0\,0\,2)}$	β (rad)	D_m (nm)
	Drying temperature	Annealing temperature				
1	350	700	34.504	5057	0.00314	46.2
2	350	750	34.542	6487	0.00291	49.9
3	350	850	34.543	3910	0.00305	47.6
4	400	700	34.542	8107	0.00319	45.5
5	400	750	34.543	7500	0.00300	48.4
6	400	850	34.521	9591	0.00302	48.1
7	450	700	34.543	2796	0.00329	44.1
8	450	750	34.544	2747	0.00312	46.5
9	450	850	34.523	2696	0.00274	53.0

In general, high-temperature treatment leads to enhanced *c*-axis orientation and a larger grain size compared with low-temperature processing [19]. However, the overall peak intensities of the films dried at 450 °C are the lowest among the three dry temperatures, so we rule out the dry temperature of 450 °C as the optimal one. The peak intensities are commonly the highest when the ZnO thin films were dried at 400 °C compared with the other dry temperatures. Focusing on the three XRD results with dry temperature of 400 °C, we found that the minimum FWHM of the (0 0 0 2) peaks was acquired when the ZnO thin film was annealed at 750 °C, showing that the improvement in the crystalline quality of the films annealed at 750 °C.

All the results above suggest that appropriate heat treatment (dry temperature 400 °C, annealing temperature 750 °C in our experimental) could effectively induce the growth of highly *c*-oriented ZnO films. In addition, a comparison of XRD Omega rocking curve around (0 0 0 2) peak between the dry temperature of 350 °C and 400 °C further proves that the latter is better, as shown in Fig. 1(c) and (d).

Chemical bath deposition based on seed layer is in common use on preparing nanostructures [20]. Seed layer is one of the important factors for the formation of ZnO nanostructures, and the template layer was spin coated for just one time, with a thickness about ~30 nm. From the SEM images as shown in Fig. 2, besides the ZnO nanorods grown vertically on the seed layer, large quantities of ZnO microrods with averaged diameter of about 4 μm randomly lay on the well-aligned nanorods. The larger microrods appeared in Fig. 2(c) and (d) should be derived from the solution, including the microrods nucleation process. In the CBD solution, the main chemical process can be described as [13]:

$$(CH_2)_6N_4 + 6H_2O \leftrightarrow 6HCHO + 4NH_3, \quad (2)$$

$$NH_3 + H_2O \leftrightarrow NH_4^+ + OH^-, \quad (3)$$

$$OH^- + Zn^{2+} \leftrightarrow Zn(OH)_2 \leftrightarrow ZnO(s) + H_2O. \quad (4)$$

The growth of ZnO involves homogeneous and heterogeneous crystallizations, which occurs simultaneously and competitively. The former results in randomly distributed ZnO microrods with large diameter, whereas the latter develops into well-aligned ZnO nanorods on the seed layer. The results of UV-Vis-NIR optical absorption and laser particle size analysis concerning the solution exhibited detailed growth kinetics of the CBD solution itself. Fig. 3(a) shows the optical absorption spectra through the solutions (HMT + $Zn(Ac)_2$, 0.025 M, respectively) after different heating time. In particular, there is a peak around ~375 nm in the optical absorption spectrum, which is corresponding to the band gap of ZnO (3.37 eV), illustrating that ZnO crystalline grew and dispersed within the mother solution well enough to be detected by the absorption measurement. Fig. 3(b) shows the results of

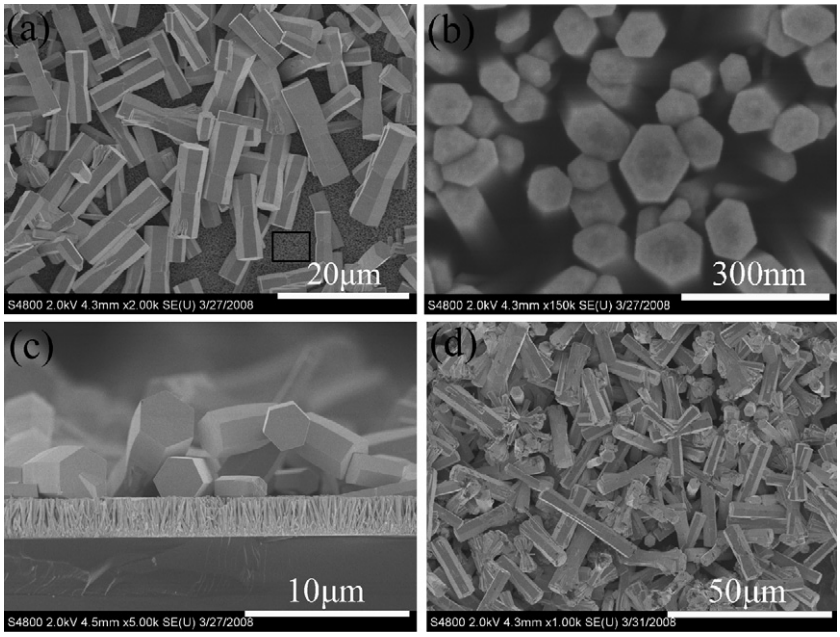

Fig. 2. SEM images of the film with the seed layer face up (a and c); (b) enlarged SEM image of the rectangle area shown in (a); (d) ZnO microrods directly on the upper surface of bare glass without any seed layer.

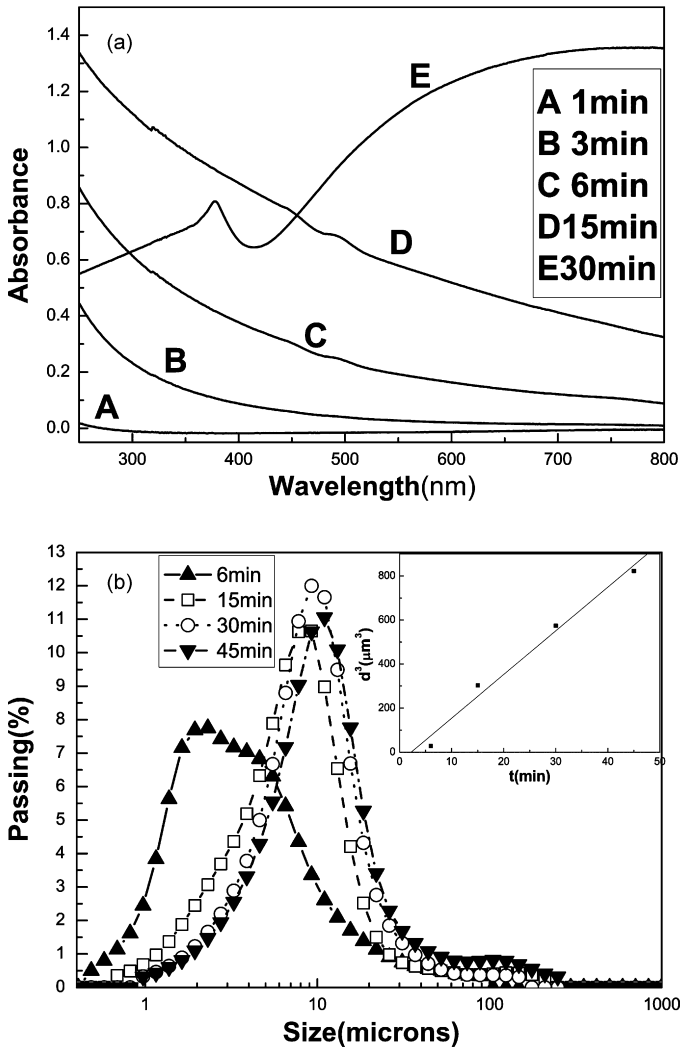

Fig. 3. (a) Optical absorption spectrum through the CBD solutions with different heating time, (b) laser particle size analysis for the same solutions; inset of (b): the dependence of the cubic of the averaged diameter of ZnO particles on the heating time.

laser particle size analysis for the same solution, revealing that the particle size in the solution is getting larger with the heating time. Although laser particle size analysis just provided statistics and three dimension-related diameter results, we still tentatively plotted a curve, the dependent of the cubic of the averaged diameter of the ZnO crystal on the heating time, which follows the expected $d \propto t^{1/3}$ law, where t and d are the time and averaged diameter of ZnO crystal, respectively, as seen distinctly in the inset to Fig. 3(b). The dependence of crystal size on the time is quantitatively matching with the so-called Ostwald ripening mechanism [21], a reactants transportation-limited growth process, which believes that the reactants-diffusion process is a decisive parameter to govern the crystal growth. Actually, this crystal growth model is too simplified to describe all the crystal growth processes involved in the complicated system in this case. The following paragraph would make further discussion.

The averaged difference in diameter between the randomly grown microrods and well-aligned nanorods present on the same specimen is pronounced, i.e., 4 μm for the microrod while 90 nm for the nanorod. The calculated values of the averaged growth speed in term of $\sim 4 \times 10^{-7}$ mg/h for the microrod and $\sim 6 \times 10^{-11}$ mg/h for the nanorod, respectively, exhibit 4 orders of magnitude in difference.

Why both the diameter and the growth speed differ notably for the vertically grown ZnO nanorod and randomly grown microrod? First of all, the microrods have a little longer growth time, 10 min at most compared to the nanorods because the precipitation process in the mother solution occurred almost immediately upon mixing and heating the CBD solution [22,23]. Premixing the equi-molar of zinc acetate and HMT before inserting substrate would induce considerable nanoparticle precipitation in the solution. The solution provides the source of crystal growth while the isoperibol bath gives the dynamic force for crystal growth in the chemical process [24]. The crystals of the microrods are initially small in size, and grow rapidly with the time. Once approaching the critical size, the microrods wend down eventually due to gravity, which was visually observed that some white powder-like things present both on the surface of ZnO pre-coated substrate with face up configuration and on the bottom of the reaction beaker. From the quantity point of view, the mean volume and mass for the microrod is 1.6×10^{-7} cm^3 (from the volume only it can be deduced that the movement of large microrods are out of the range of Brownian motion) and 8.7×10^{-7} mg, respectively, and the buoyancy and the gravity of the microrod is 1.5×10^{-9} N and 8.6×10^{-9} N, respectively, verifying that the quantitative difference between the mass and buoyancy of the ZnO microrod. Such microrods as seen in Fig. 2(c) were orientated in an arbitrary fashion, and the well-defined crystallographic faces, i.e., polar (0 0 0 1) and non-polar (0 1 $\bar{1}$ 0) faces, can be identified clearly and distinctively. However, when the substrate was put vertically with respect to liquid level or with seed layer face down, the large microrods lying onto the nanorods were absent, as shown in Fig. 4(c) and (d). Actually the big size ZnO microrods still formed on the bottom of the beaker irrespective of how to insert the substrate.

Secondly and more importantly, the introduced seed layer was expected to change the growth fashion in the solution. The nuclei site density on the seed layer is superior to that in the solution. The template layer already has either positively or negatively charged surface of ZnO, which can govern ZnO nanorods growth. However, for the case of nuclei sites in the mother solution, small amounts of contaminants in the reagents would facilitate the formation of in situ CBD nucleation centers, regardless of the presence or absence of any seed layer [25]. ICP elemental analysis of unpurified reagents revealed the presence of Fe (21 ppm) and Pb (15 ppm) in the CBD mother solution. The hydroxyl complex of elemental contaminants acted as nucleation centers, resulting in rapid precipitation from the solution, which is consistent with the visual observation on the bottom of the beaker. One can envisage that there are countless polar surfaces on the pre-coated seed layer, while the in situ CBD solution nucleation centers are relatively less partially due to the contaminants in ppm level. Hereby, there is higher nucleation density on the seed layer than that in the mother solution, which in turn causes a faster and competitive consumption of Zn ions near the nucleation sites on the seeded surface. Analogous to the concentration gradient between the bulk solution and the distal one, the local concentration of Zn^{2+} and related complex close to the nuclei sites in the bulk solution (the supersaturation level of precursor was perserved) is much higher than that on the template layer, and more Zn^{2+} could be diffused to in situ nucleation centers in the bulk solution, leading to the prevailing growth of homogeneous crystallization.

The diameter roughly had 44-fold difference between microrods and nanorods although the growth time lag between them is 10 min at most in our experiment. As mentioned above, the growth of microrods followed well with the diffusion-limited "Ostwald ripening" mechanism, but nevertheless it can be expected that the Ostwald ripening theory only cannot account for the growth of well-aligned nanorods with respect to the huge 44-fold difference

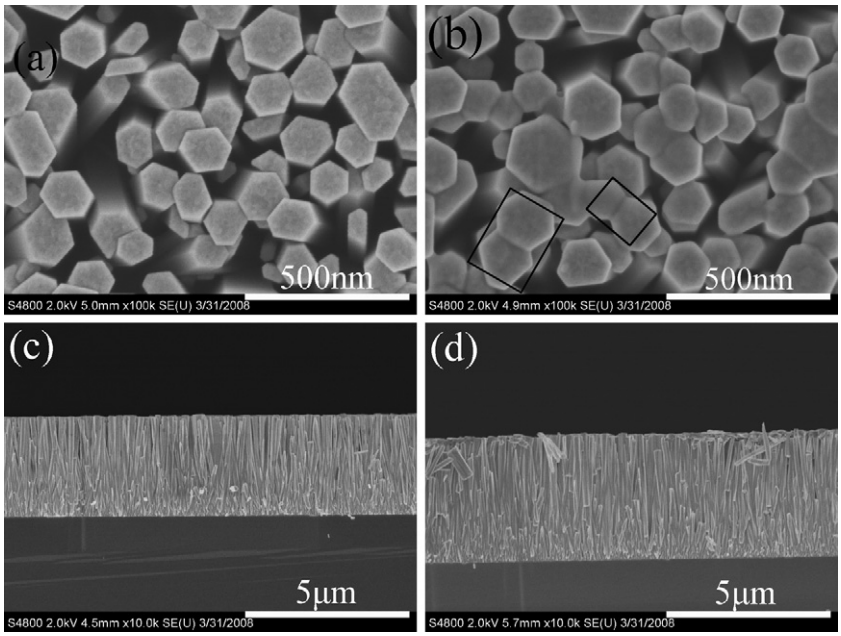

Fig. 4. Nanorods grown on the seed layer, surface morphologies: (a) the substrate was vertically standing and (b) the seed layer was faced down; cross-sectional morphologies (c) the substrate was vertically standing, (d) the seed layer was face down.

in diameter. Viswanatha et al. [21] studied the growth kinetics dependence on the temperature as well as the reactant concentration, suggesting that the too simplified "Ostwald ripening" model invalidates to interpret heterogeneous growth. For the well-ordered ZnO nanorods on the seed layer formed in the CBD process, both the diffusion of Zn^{2+} ions and the reaction at the surface of the crystalline to incorporate the reactants have to be taken into consideration to model the nanorod growth, i.e., the growth

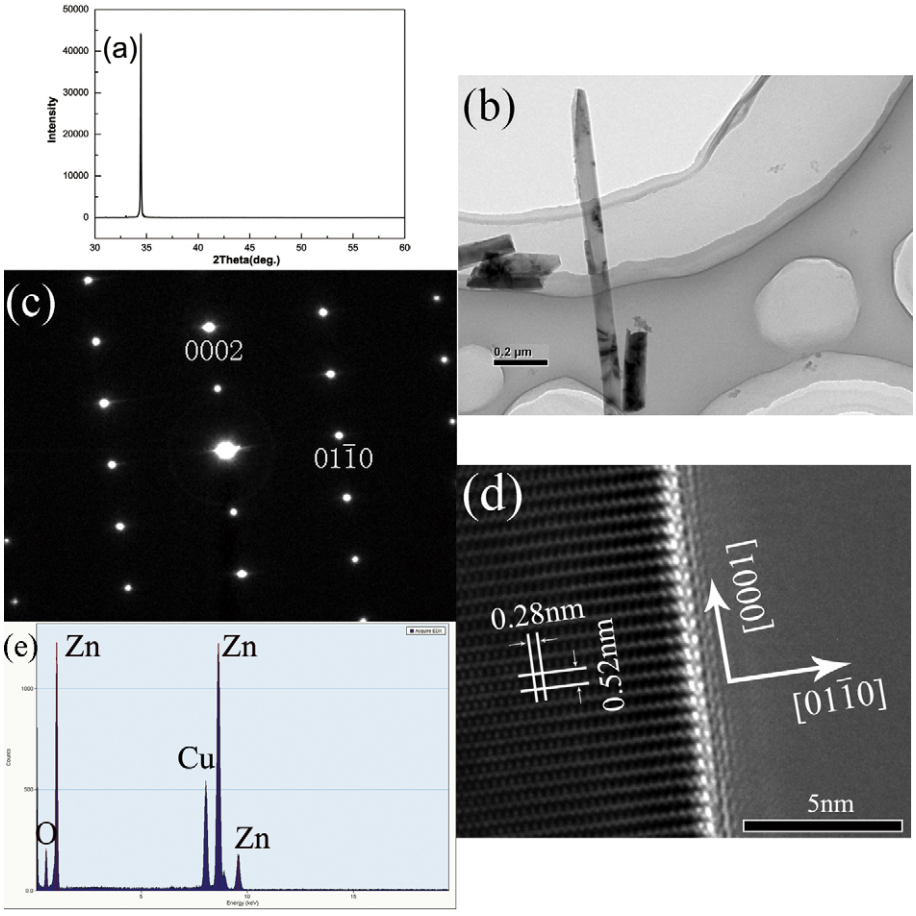

Fig. 5. (a) XRD pattern of the sample that were placed vertically, (b) TEM, (c) SAED pattern, (d) HRTEM image and (e) EDX image of the nanorod from the same specimen.

kinetics of the nanorods rely on the temperature, the growth time, the local reactant concentration as well as the reaction kinetics on surface energy driven effects.

Well-aligned ZnO nanorod arrays were obtained by placing the pre-coated substrate vertically or horizontally with the seed layer face down, which were presented in Fig. 4. It can be seen from the cross-sectional SEM pictures that the alignment of nanorods was well ordered with high packing density. Reminiscent of Fig. 2(d), it is believed that the spin-coated ZnO film serves as a seeding layer that promotes the nucleation and subsequent growth of ZnO nanorods during the CBD process, while the blank substrate without a ZnO seeding layer yields randomly distributed ZnO microrods, arising from the homogeneous nucleation in the mother solution. There are two representative joints as seen the rectangle areas in Fig. 4(b), which exhibits that the neighbor nanorods grown in a direction deviating from the rigid vertical growth azimuth would fuse together, and finally combine into one nanorod with a large diameter. The coalescence of adjacent nanowires rendered objective evidence to the issue reported by Li et al. [26]. In the future studies, it is highly desirable that nanorod diameter, length, spacing and orientation could be tuned proactively by changing the growth time, solution concentration, or the nature of seed layer.

Further attention upon the microstructure of the ZnO well-ordered nanorod arrays is paid by using XRD and (HR) TEM. The results are exhibited in Fig. 5. In the XRD pattern, only (0 0 0 2) peak of wurtzite ZnO with narrow FWHM was observed, other peaks such as $(1\,0\,\bar{1}\,0)$, $(1\,0\,\bar{1}\,1)$, $(1\,0\,\bar{1}\,2)$, etc. were absent, quite different from the previously reported hydrothermal results [27], which indicates that the wurtzite ZnO nanorods are highly orientated and have epitaxial relationship with the ZnO seeding layer. The microstructure of the material has also been investigated by employing TEM, SAED pattern and HRTEM. The SAED pattern taken along $[2\,\bar{1}\,\bar{1}\,0]$ zone axis means that the nanorod has (0 0 0 1) top and bottom surfaces. The fastest growth direction is along the *c*-axis. The HRTEM image in Fig. 5(d) shows well-defined two-dimensional (2D) lattice planes and demonstrates the good crystallinity of the nanorods, without any dislocations and stacking faults. The lattice planes with spacing of 0.52 and 0.28 nm correspond to the (0 0 0 1) and $(0\,1\,\bar{1}\,0)$ planes, respectively. In addition, an energy dispersive X-ray spectroscopy (EDX) attached to the TEM was utilized to check the composition of the nanorod. Only zinc and oxygen were detected. The characteristic of Cu peak comes from the copper grid. As shown in Figs. 4 and 5, the hexagonally shaped nanorods uniformly covered the ZnO-coated substrate with high density, featuring good alignment and *c*-axis preferred orientation. For the former, we suggest that the reason for superior alignment is due to both lattice matching and polar nature of the ZnO surface. ZnO surface is either positively or negatively charged. In either case the surface will attract opposite charged ions to it and react to form ZnO nanorods. Thus the ZnO seeding layer plays an important role in achieving high density of ZnO nanorod arrays. For the latter, the fastest growth direction is along the *c*-axis because of the presence of highly polar oxygen and zinc atoms along the [0 0 0 1] direction. High crystalline quality of ZnO nanorods can be successfully synthesized at rather low temperature (90 °C in this case) through all solution processes, which is attractive both for scientific exploration and application-driven demands.

Fig. 6 depicts the photoluminescence spectrum of a sample that the substrate was placed vertically with respect to the solution liquid level, which was excited with a laser (325 nm) at room temperature. As can be seen in this diagram, the PL spectrum mainly includes two peaks: a near band edge (NBE) emission centered at about 380 nm and a deep-level (DL) emission band around 550 nm [28]. The NBE emission is in good agreement with the typically reported free excitation emission, and the DL emission could be attributed to some oxygen vacancies or zinc interstitials present in the host matrix [29].

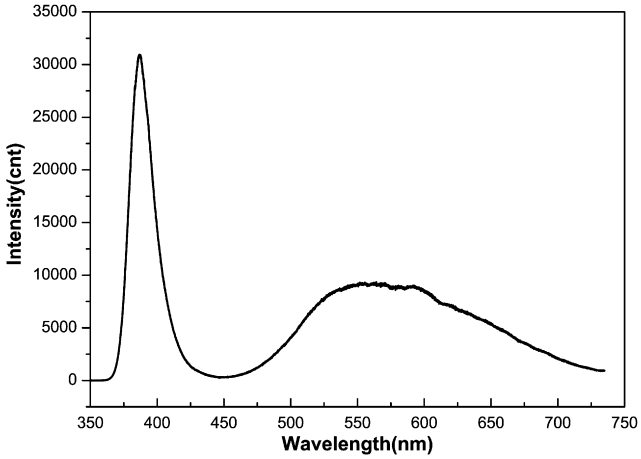

Fig. 6. PL spectrum of the sample at room temperature.

4. Conclusions

In conclusion, chemical bath deposition combined with sol–gel method was utilized to grow ZnO nanostructures. Well-aligned ZnO nanorod arrays were grown vertically onto the ZnO pre-coated layer, following heterogeneous nucleation and growth mechanism, while randomly distributed ZnO microrods were produced simultaneously, featuring homogeneous growth mode. Well-aligned ZnO nanorods were successfully synthesized on the *c*-oriented ZnO seed layers, which were produced on silicon substrates with the optimized sol–gel and spin-coating procedures. Structural analysis revealed that the ZnO nanorod arrays are single crystalline in nature and grow along *c*-axis direction. The PL spectrum showed a sharp UV emission and a broad green emission, deriving from excitonic transitions of the band gap and point defects, respectively.

The heterogeneous and homogeneous crystallization co-exist in the same hydrothermal reaction, and compete with each other. Approximate 4 orders of magnitude difference in growth speed between microrods and nanorods was observed. ZnO microrods could grow faster with less nuclei site density and relatively more diffused Zn^{2+} source available. The growth of microrods followed well with the diffusion-limited "Ostwald ripening" mechanism, while the growth of well-aligned nanorods is not only limited by the diffusion, but also by the temperature, the growth time, density of nuclei site as well as local reactant concentration.

Acknowledgments

This work was supported by Ningbo Natural Science Foundation, China (Grant no. 2008A610052). We are grateful to Dr. Zhaoping Liu for his valuable discussion.

References

[1] U. Rössler, Phys. Rev. 184 (1969) 733.
[2] R. Könenkamp, R.C. Word, C. Schlegel, Appl. Phys. Lett. 85 (2004) 6004.
[3] R.M. Wang, Y.J. Xing, J. Xu, D.P. Yu, New J. Phys. 5 (2003) 115.
[4] Y.B. Li, Y. Bando, T. Sato, K. Kurashima, Appl. Phys. Lett. 81 (2002) 144.
[5] W.I. Park, D.H. Kim, S.W. Jung, G.C. Yi, Appl. Phys. Lett. 80 (2002) 4232.
[6] M.H. Huang, S. Mao, H. Feick, H. Yan, Y. Wu, H. Kind, E. Weber, R. Russo, P. Yang, Science 292 (2001) 1897.
[7] Q.H. Li, Y.X. Liang, Q. Wan, T.H. Wang, Appl. Phys. Lett. 85 (2004) 6389.
[8] J. Goldberger, D.J. Sirbuly, M. Law, P.J. Yang, Phys. Chem. B 109 (2005) 9.

[9] S. Ju, K. Lee, D.B. Janes, M.H. Yoon, A. Facchetti, T.J. Marks, Nano Lett. 5 (2005) 2281.
[10] Y.W. Heo, V. Varadarajan, M. Kaufman, K. Kim, D.P. Norton, F. Ren, P.H. Fleming, Appl. Phys. Lett. 81 (2002) 3046.
[11] K. Govender, D.S. Boyle, P. O'Brien, D. Binks, D. West, D. Coleman, Adv. Mater. 14 (2002) 1221.
[12] Y. Li, D.W. Meng, L.D. Zhang, F. Phillipp, Appl. Phys. Lett. 76 (2000) 2011.
[13] S. Yamabi, H. Imai, J. Mater. Chem. 12 (2002) 3773.
[14] R.B.M. Cross, M.M.D. Souza, E.M.S. Narayanan, Nanotechnology 16 (2005) 2188.
[15] Y. Sun, G.M. Fuge, N.A. Fox, D.J. Riley, M.N.R. Ashfold, Adv. Mater. 17 (2005) 2477.
[16] L.L. Yang, Q.X. Zhao, M. Willander, J.H. Yang, J. Cryst. Growth 311 (2009) 1046.
[17] L.L. Yang, Q.X. Zhao, M. Willander, J.H. Yang, I.G. Ivanov, J. Appl. Phys. 105 (2009) 053503.
[18] L.L. Yang, Q.X. Zhao, M. Willander, J. Alloys Compd. 469 (2009) 623.
[19] J.H. Lee, K.H. Ko, B.O. Park, J. Cryst. Growth 247 (2003) 119.
[20] Y.F. Gao, M. Nagai, Langmuir 22 (2006) 3936–3940.
[21] R. Viswanatha, K. Santra Pralay, C. Dasgupta, D.D. Sarma, Phys. Rev. Lett. 98 (2007) 255501.
[22] J.H.K. Kim, E.-M. Kim, D. Andeen, D. Thomson, S.P. DenBaars, F.F. Lange, Adv. Funct. Mater. 17 (2007) 463–471.
[23] W.J. Li, E.W. Shi, W.Zh. Zhong, Zh.W. Yin, J. Cryst. Growth 203 (1999) 186–196.
[24] M. Ethayaraja, R. Bandyopadhyaya, Langmuir 23 (2007) 6418–6423.
[25] M. Kokotov, A. Bicler, G. Hodes, Chem. Mater. 20 (2008) 4542.
[26] Z.K. Li, X.T. Huang, J.P. Liu, Y.Y. Li, G.Y. Li, Mater. Lett. 62 (2008) 1503–1506.
[27] M. Guo, P. Diao, S. Cai, J. Solid State Chem. 178 (2005) 1864.
[28] Y. Li, G.W. Meng, L.D. Zhang, F. Phillipp, Appl. Phys. Lett. 76 (2000) 15.
[29] P. Sagar, P.K. Shishodia, R.M. Mehra, H. Okada, A. Wakahara, A. Yoshida, J. Lumin. 126 (2007) 800–806.